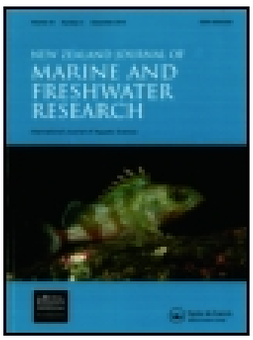

New Zealand Journal of Marine and Freshwater Research

ISSN: 0028-8330 (Print) 1175-8805 (Online) Journal homepage: http://www.tandfonline.com/loi/tnzm20

Wave climate of the western Bay of Plenty, New Zealand, 1991–93

Graham H. Macky , Geoff J. Latimer & R. Keith Smith

To cite this article: Graham H. Macky , Geoff J. Latimer & R. Keith Smith (1995) Wave climate of the western Bay of Plenty, New Zealand, 1991–93, New Zealand Journal of Marine and Freshwater Research, 29:3, 311-327, DOI: 10.1080/00288330.1995.9516666

To link to this article: http://dx.doi.org/10.1080/00288330.1995.9516666

New Zealand Journal of Marine and Freshwater Research, 1995, Vol. 29: 311–327
0028–8330/95/2903–0311 $2.50/0

Wave climate of the western Bay of Plenty, New Zealand, 1991–93

GRAHAM H. MACKY
National Institute of Water & Atmospheric Research Ltd
P. O. Box 8602
Christchurch, New Zealand

GEOFF J. LATIMER
R. KEITH SMITH
National Institute of Water & Atmospheric Research Ltd
P. O. Box 11–115
Hamilton, New Zealand

Abstract Wave measurements were made for 3 years from a buoy moored in 34 m water depth off the Katikati inlet in the western Bay of Plenty, New Zealand. The significant wave heights were less than 1 m for 70% of the time, with a mean of 0.8 m, and a maximum of 4.3 m. The peak in the spectral density occurred each year at 0.09–0.10 Hz (10–11 s period). Wave steepness suggests that many of the measured waves originated close to the buoy. The year-to-year uniformity in averaged spectral density masks considerable short-term variability although there is some evidence of higher wave energy in winter. Most wave energy arrived from the north-east to east sector. Calculations of the longshore wave energy flux factor suggest that the direction of littoral drift fluctuates frequently, but during the 3 years studied there was a small nett drift in a north-west direction. Significantly less wave energy was measured at Katikati than in previous studies at Great Barrier Island and Hicks Bay. Our Katikati wave data may not be typical of the long-term climate, because they were obtained in El Niño conditions when fewer storms occur.

M94062
Received 25 November 1994; accepted 1 June 1995

Keywords short-period waves; wave spectra; buoy measurements; wave climate; sediment transport

INTRODUCTION

Wave data relevant to the Bay of Plenty are limited, comprising mostly short-duration records measured in different places using a variety of techniques. Shore-based observations of breaker height, wave direction, and longshore current were made for about 1 year at Waihi Beach (Fig. 1) by Harray (1977) and at Whiritoa Beach by Christopherson (1977); Davies-Colley (1976) reported observations made from the pilot boat at the entrance to Tauranga Harbour. de Lange (1991) described a record (1989–91), of wave height and period measured in shallow water (13 m water depth) off the Port of Tauranga using a recording pressure transducer. More recent measurements were made at the same site using an InterOcean S4 recording current meter. Wave rider buoy deployments in deep water (60 m) were made near Hicks Bay (Fig. 1) over a 9-month period in 1978–79 (Harris et al. 1983) and for 2 years in 1980–81 to the east of Great Barrier Island in deep water (65 m) (Ewans & Coup 1982; Ewans & Kibblewhite 1992). The only long-term records come from the routine observations of sea and swell climate in deep water made by coastal shipping in the Auckland-Poverty Bay region (e.g., Reid & Collen 1983), but these data must be used with caution because of inaccuracies in the estimation methods and because observations were made at random over a very large area.

In summarising data from various sources (predominantly shore-based observations), Pickrill & Mitchell (1979) characterised the wave climate in the northern (east coast) region of New Zealand as follows. Waves are generally smaller than elsewhere on the New Zealand coast. The prevailing deep-water waves approach the coast from directions ranging between north and east with a wave height of 0.5–1.5 m and a wave period of 5–

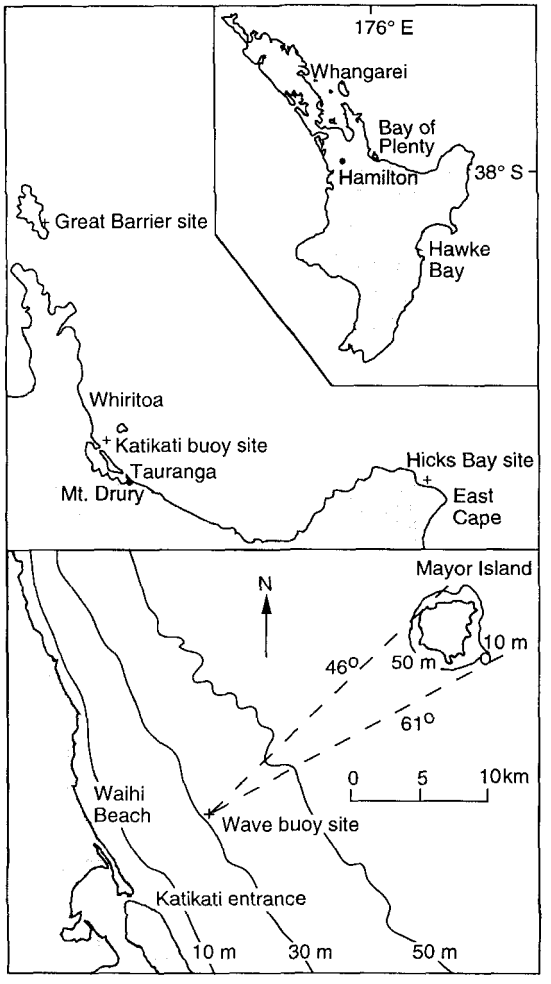

Fig. 1 Location map of Bay of Plenty, North Island, New Zealand indicating wave buoy site and isobaths.

7 s whereas at the beach waves are typically 0.4–0.8 m high with a period of 9–12 s. Long-period swells appear to originate from subtropical disturbances north of New Zealand whereas shorter-period seas are generated by local weather patterns. Pickrill & Mitchell suggested that a slightly higher frequency of storms in winter causes a weak seasonality in the wave climate. In the shallow waters off Tauranga Harbour, de Lange (1991) observed a persistent oceanic swell (mean height about 0.3 m, period 12–16 s) with locally generated shorter-period waves superimposed. Although no strong seasonal pattern was evident, he subsequently reported a long-term trend associated with the southern oscillation (Hume et al. 1992).

In February 1991 the National Institute of Water and Atmospheric Research Ltd (NIWA) installed a directional wave measuring buoy off the Katikati inlet in the western Bay of Plenty, as part of a study of sediment movement in the region. This paper reports the results of analysis of the first 3 years of data, describes the wave characteristics and discusses the implications for the wave climate and sediment transport in the western Bay of Plenty.

DATA ACQUISITION

The buoy site

The buoy was deployed at the base of the shoreface in 34 m water depth 8 km off the Katikati entrance to Tauranga Harbour (37°24.837′S, 176°03.238′E, see Fig. 1). This site, adjacent to the wreck of the SS *Taupo*, afforded protection from trawler strike.

The ENDECO buoy and data processing

The wave buoy is an ENDECO Wave-track (Model 1156) instrument which was programmed to record for 17 min every 3 h. The buoy transmits data by radio signal 26 km down-coast to the Port of Tauranga signal station at Mt Drury where data are logged on a PC and relayed to NIWA in Hamilton.

The buoy is 2 m long and rides vertically in the water, tethered to the seabed by a flexible mooring. The buoy's sensor package sits 1.5 m below the water surface and contains an accelerometer, X-tilt and Y-tilt sensors, and flux gate compass. The accelerometer measures vertical motion and the measured acceleration is integrated twice to obtain vertical displacement, a method standard in wave measuring buoys. To detect wave direction, the buoy's tilt is measured in north-south and east-west directions. The software provided by ENDECO uses the tilt information to compute directional spread and a mean direction for each frequency component. An earlier model of the ENDECO buoy was compared with other instruments by Allender et al. (1989) who found ENDECO's estimates of directional spread to be unrealistic. Given this uncertainty we have chosen to ignore the directional spread measurements and use only the mean direction. This mean direction was obtained by weighting the mean direction for each frequency component by the energy density for that component (Appendix I). For records associated with significant wave energy, mean directions calculated this way matched the window

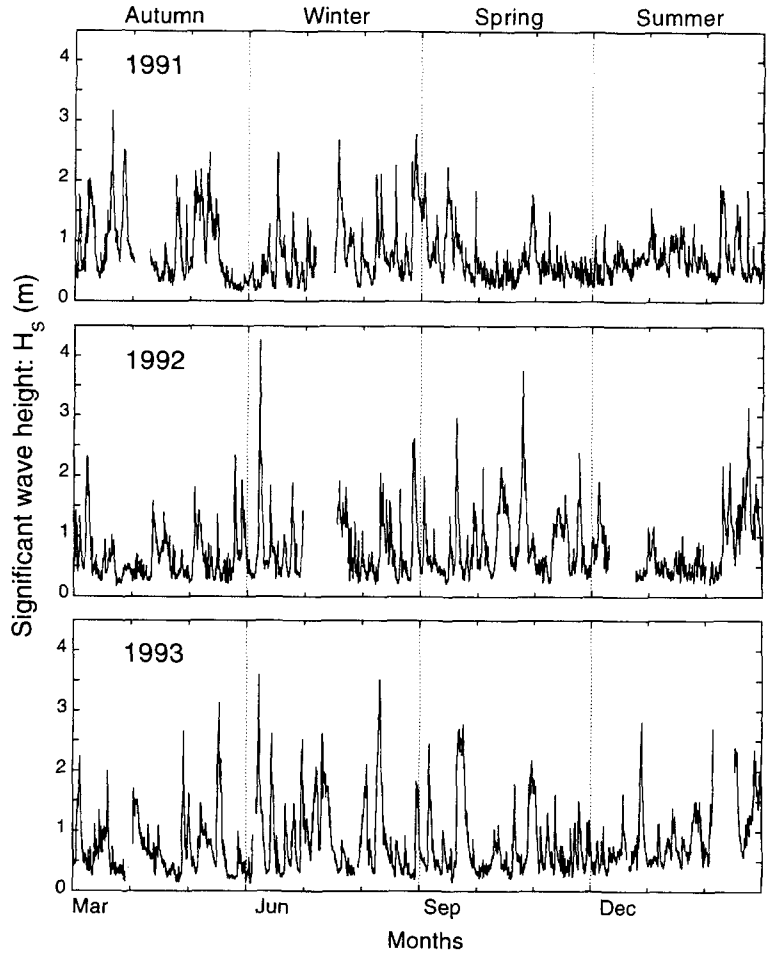

Fig. 2 Significant wave height (H_s) for period 1991–93. Seasons represent 3-monthly data: March-May, June-August, September-November, and December-February, inclusive. Years represent March to February (following year) inclusive.

of open sea. This offered us some assurance that the mean directions were valid.

To summarise the wave climate we estimated the following standard parameters from the wave record: significant wave height, H_s; significant wave period, T_s; and spectral peak period, T_p. These parameters were estimated using ENDECO software which includes zero-crossing and spectral analysis (Appendix 1). We also calculated spectral densities (summed across all directions) which we averaged over time (by season and year). In order to make inferences about the patterns of longshore sediment transport in the littoral zone resulting from the incident waves, we calculated the total wave energy flux factor per unit length of shoreline and its longshore component, from H_s, T_p and mean wave direction using equations in the Shore Protection Manual (USCERC 1984) (see Appendix 1).

RESULTS

Wave height and period

The time series of significant wave height over the record period is shown in Fig. 2. The two largest storms occurred in June and October 1992 and the highest significant wave height recorded was 4.3 m. A notable feature was the absence of significant storm events during the period October 1991 to January 1992 although this pattern was not repeated in the subsequent 2 years. The frequency distributions of significant wave height H_s for the 3 years were similar (Fig. 3): significant wave

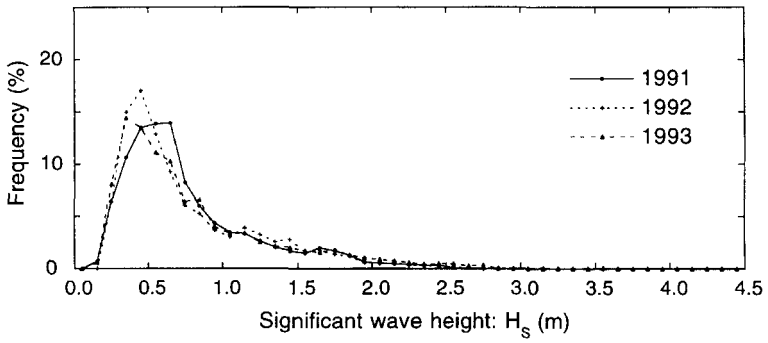

Fig. 3 Annual significant wave height (H_S) distribution at 0.1 m height intervals.

heights were less than 1 m for about 70% of the time and the mean wave heights were about 0.8 m in all 3 years although the modal wave heights differed; 0.7, 0.5, and 0.4 m in 1991, 1992, and 1993 respectively. There were differences between seasons (Fig. 4) with significant wave heights exceeding 1.2 m more often in all three winters and in Autumn 1991 and Spring 1992. The modal value for significant wave height in Summer 1991/92 was 0.7 m, above average in spite of a dearth of large waves (see Fig. 2), indicating that background wave activity was higher than usual. Table 1 gives summary statistics of wave height and period for each year: despite the seasonal differences noted above, mean values for the 3 years were similar.

Significant wave period T_S is plotted against significant wave height H_S in Fig. 5, which also shows the individual distributions of H_S and T_S for the entire record. Graphs for individual years and seasons were similar and are not presented. The mean value of T_S was 6 s, and for any given value of H_S there was a wide range of wave periods. We can use Fig. 5 to make inferences about the origin of the measured waves. The Shore Protection Manual (USCERC 1984) presents equations for H_S and T_S in a fully-arisen sea which can be combined to give:

$$H_S/(g\ T_S^2) = 0.00408 \quad (1)$$

Equation 1 is plotted in Fig. 5, and defines for the fully-arisen sea the maximum wave height for a given wave period (i.e., the maximum wave steepness) above which wave breaking occurs. $H_S/(g\ T^2)$ can be regarded as a measure of wave steepness, and (in a fully arisen sea) wave breaking prevents the occurrence of values exceeding the value of 0.00408 given by Eqn 1. The Shore Protection Manual also presents equations for H_S and T_S in developing seas, and these equations can be manipulated to show that $H_S/(g\ T^2)$ then does exceed this value. This was the situation for many of the measured waves (those lying above the line in Fig. 5), suggesting that on those occasions waves were generated close to the buoy, probably within about 500 km. For a large number of waves $H_S/(g\ T^2)$ was much less than 0.00408, indicating either that these waves originated some distance from the buoy and had decayed significantly before reaching the buoy, or that they were measured at the end of a storm when the sea was abating.

Figure 6 shows the cumulative probability distribution of significant wave height plotted on a log scale to emphasise extreme events. It shows, for example, that H_S exceeded 4 m for 0.008% of the time. It is tempting to extrapolate the curve in Fig. 6 to estimate wave heights for extreme events such as the 100-year storm. However, this cannot

Table 1 Range of wave height and period in individual years.

		1991–92	1992–93	1993–94
H_{max} (m)	Maximum	4.98	6.69	6.01
	Mean	1.28	1.29	1.32
	Minimum	0.25	0.34	0.25
H_s (m)	Maximum	3.16	4.27	3.59
	Mean	0.77	0.77	0.80
	Minimum	0.15	0.17	0.13
T_z (s)	Maximum	12.55	11.41	12.03
	Mean	5.91	5.83	6.05
	Minimum	2.82	2.91	2.76
T_s (s)	Maximum	13.72	12.45	13.60
	Mean	6.12	6.03	6.30
	Minimum	2.15	2.25	2.34
T_p (s)	Maximum	16.66	16.66	20.00
	Mean	9.08	8.88	9.22
	Minimum	1.81	2.22	2.00

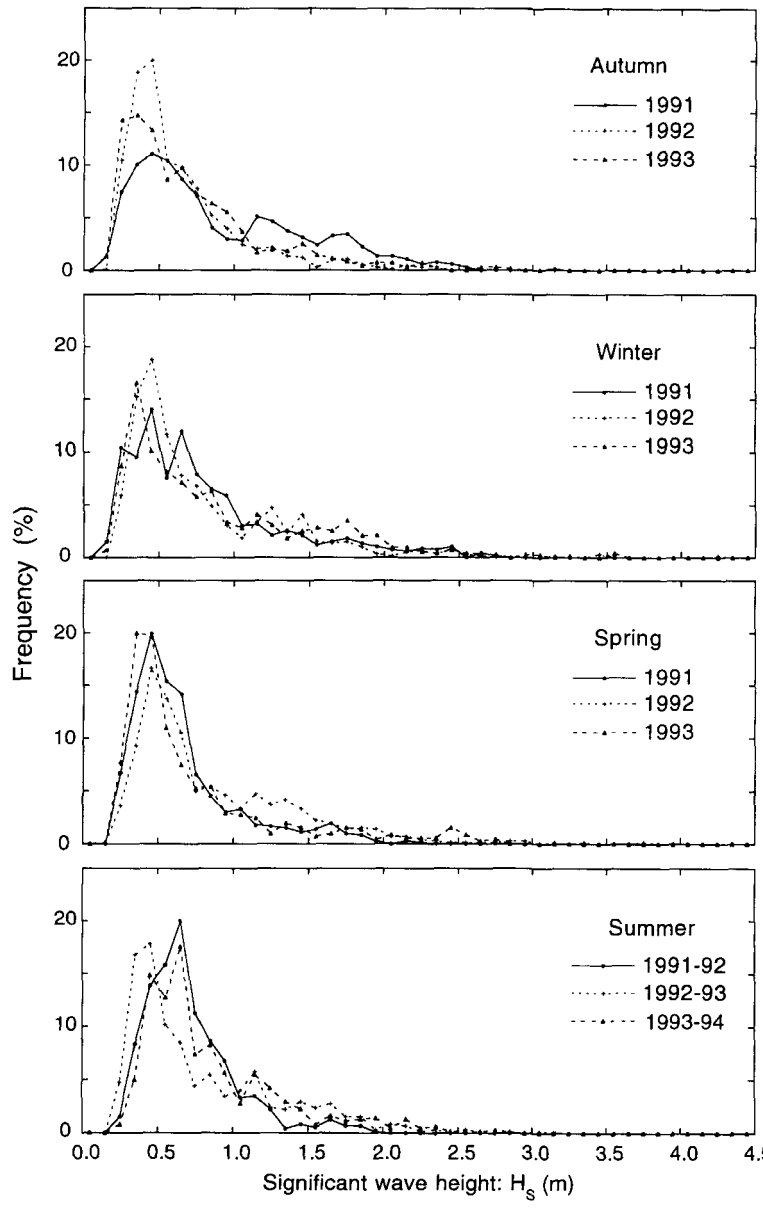

Fig. 4 Seasonal significant wave height (H_S) distribution at 0.1 m height intervals.

be done with confidence because a 3-year record is not long enough to make reliable predictions about extreme events and the 3 years studied may not be representative of the long-term climate (see discussion below about the Southern Oscillation).

Averaged spectral densities

The distributions of wave energy by frequency band (spectral density) at the buoy site for each of the 3 years are shown in Fig. 7. The area under each curve is proportional to the total wave energy. Little year-to-year variation is apparent, either in the total wave energy or the shape of the energy spectrum, and the spectral peak occurred consistently at frequencies in the range 0.09–0.10 Hz (period 10–11 s). Fig. 8, however, which compares the spectral densities for individual seasons with the 3-year average spectral density,

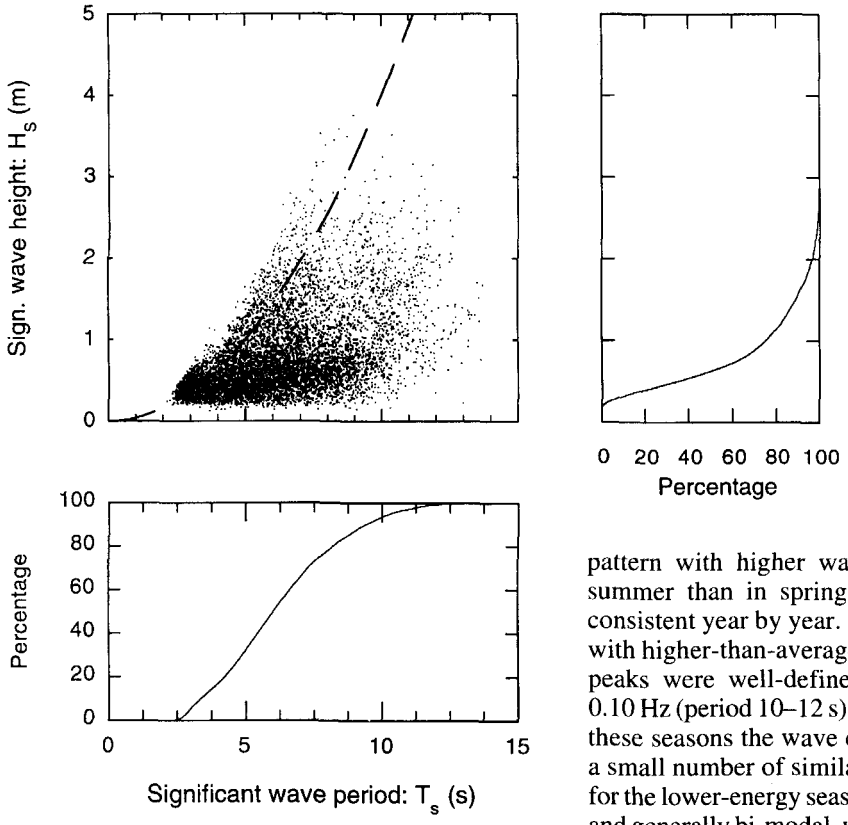

Fig. 5 Scatter plot of significant wave height (H_s) versus significant wave period (T_s) for the period 1991–93 and cumulative distributions of H_s and T_s. The dashed line represents a fully arisen sea as computed from formulae in USCERC (1984).

indicates that this year-to-year uniformity masks considerable short-term variability. Except perhaps in winter, in none of the four seasons was wave energy consistently higher or lower than the 3-year average. For example, in the 1991 autumn and the 1992 spring, wave energy was higher than this 3-year average, whereas in the other autumns and springs, wave energy was less than this average. Thus, although Fig. 8 suggests a weak seasonal pattern with higher wave energy in winter and summer than in spring and autumn, this is not consistent year by year. For those seasonal spectra with higher-than-average total energy, the spectral peaks were well-defined and occurred at 0.09–0.10 Hz (period 10–12 s) which suggests that during these seasons the wave climate was dominated by a small number of similar storms. By comparison, for the lower-energy seasons, the spectra were broad and generally bi-modal, which suggests waves from a mixture of sources.

Wave direction

Figure 9 shows the directional spread of mean wave energy flux factor at the buoy, for the 3 individual years. This analysis assumes that all the wave energy flux at a particular time arrives from the mean wave direction. Waves from onshore directions (145–335°), presumed to be short-period wind waves generated in the short fetch between

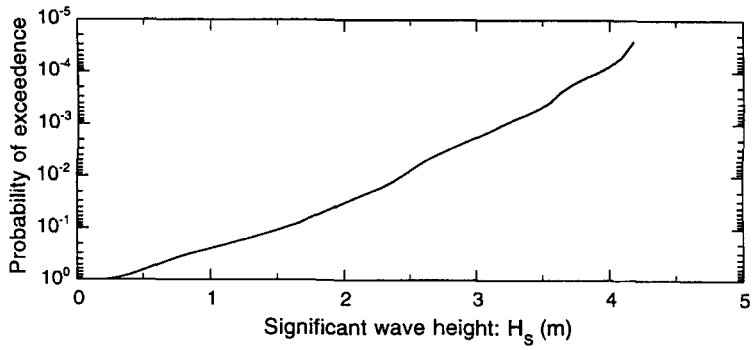

Fig. 6 Cumulative probability distribution of significant wave height (H_s) for the years 1991–93.

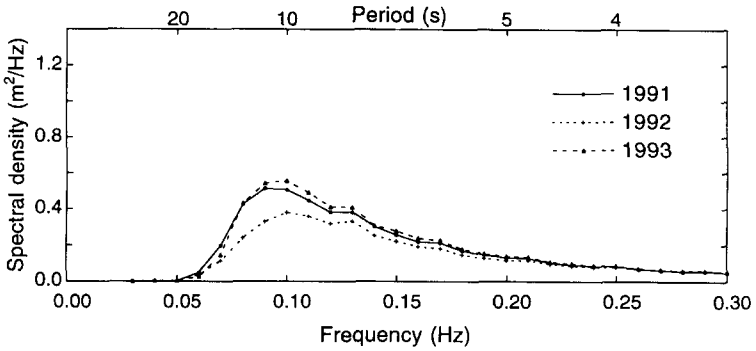

Fig. 7 Mean annual spectral densities for the years 1991–93.

the buoy and the coast, have been excluded from these calculations. It is clear that significant wave energy arrives from the entire window of open sea. The energy flux distribution has a pronounced peak in all years at 70–80°. Figure 10 shows the directional spread of energy flux factor for individual seasons and reveals wide differences between seasons. The wave flux arriving from 70–80° which dominates Fig. 9 was virtually absent in Spring 1991, Summer 1991/92, Autumn 1992, and Autumn 1993. Inspection of the time series (details omitted here) shows that the high-energy flux arriving from 70–80° is associated with a small number of major storms.

Figure 11A distributes the wave energy of the 3-year record by mean direction and frequency. The peak energy occurs at low frequencies (peak energy at 90 mHz, wave period 11 s) within the sector 60–100°. A secondary energy peak occurs at higher frequencies (peak frequency 110 mHz, wave period 9 s) and in a more northerly 20–50° band. This pattern produces a slight energy minimum at 50°. The most obvious cause of this minimum is wave sheltering by Mayor Island and reefs adjacent to it, which lie 20–25 km from the buoy at a bearing of 46–61°. However, the energy minimum varies in bearing from season to season (40° in Spring 1993, 60° in Winter 1992) (Fig. 10) and is absent in some seasons, suggesting that it may result in part from a feature of the offshore wave climate, as well as from an effect of wave sheltering. For example, in Winter 1991 there was a marked trough at 50°, with long-period energy arriving from both sides of this bearing (Fig. 11B). In contrast, in Summer 1993–94 there were high levels of long-period energy arriving from 60–90°, but also significant shorter-period wave energy associated with mean directions of around 50° (Fig. 11C). Thus the effect of Mayor Island in sheltering the buoy appears evident for longer-period waves, but is less certain for shorter periods. A numerical refraction/diffraction study, which would more precisely determine the effect of the island on the wave climate near the coast, was beyond the scope of the present paper.

Table 2 Statistics for larger recorded storms.

Date	Peak H_s (m)	Mean T_p (s)	Mean direction (degrees)
20 Mar 91	3.16	10.61	63
26 Mar 91	2.51	17.46	72
3 May 91	2.19	10.55	80
9 May 91	2.47	11.80	82
15 Jun 91	2.47	9.13	37
18 Jul 91	2.69	9.33	33
27 Aug 91	2.78	10.59	79
7 Mar 92	2.32	8.40	39
24 May 92	2.34	7.98	82
6 Jun 92	4.27	9.70	60
26 Aug 92	2.62	9.78	34
18 Sep 92	2.96	7.97	55
12 Oct 92	3.16	11.91	56
23 Oct 92	3.76	9.95	82
3 Nov 92	2.40	10.37	84
21 Feb 93	3.15	11.48	74
28 Apr 93	2.73	7.16	96
16 May 93	3.28	9.18	20
6 Jun 93	3.78	8.93	42
13 Jun 93	2.71	8.93	15
29 Jun 93	2.44	7.37	104
10 Jul 93	2.72	13.24	80
9 Aug 93	3.66	10.86	68
22 Sep 93	2.97	10.76	86
26 Dec 93	2.97	7.81	67

Storm events

Summary statistics for the 25 largest storms observed, all with significant wave heights peaking at over 2 m, are given in Table 2. Mean directions

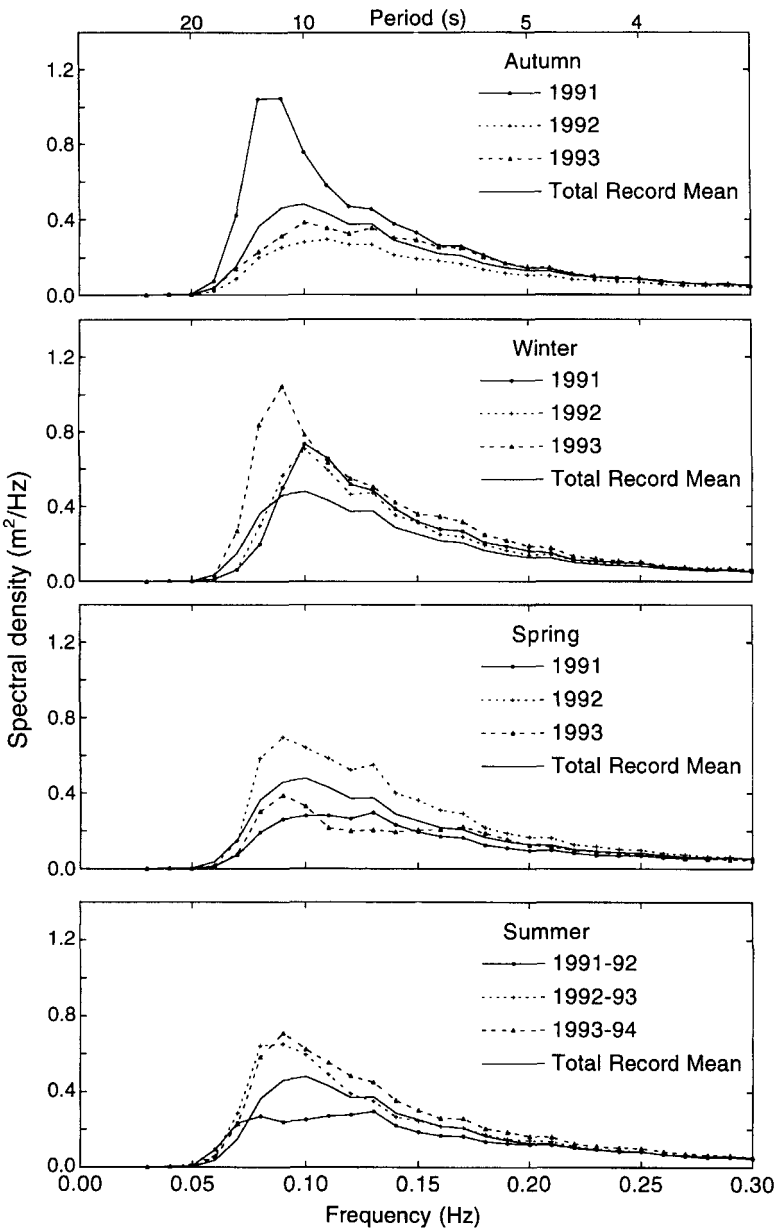

Fig. 8 Mean spectral densities for individual seasons.

ranged from 15 to 104°, but two-thirds of these events came from directions east of normal to the Waihi coast (i.e., bearings greater than 58°). Mean values of T_p ranged from 7.2 to 13.2 s. Storms with mean direction between 50 and 90° covered most of this range of periods, but T_p was between 8 s and 10 s for the 7 storms from north of 50°, and the two storms from south of 90° had the shortest periods.

Wave energy flux factors and longshore transport

Figure 12 shows time series of the daily averaged total and longshore wave energy flux factors evaluated at the breaker-line, shoreward of the wave buoy. The total wave energy flux factor is a measure of the total wave energy incident on the shore, whereas the longshore factor is a measure of the potential to transport sand alongshore within

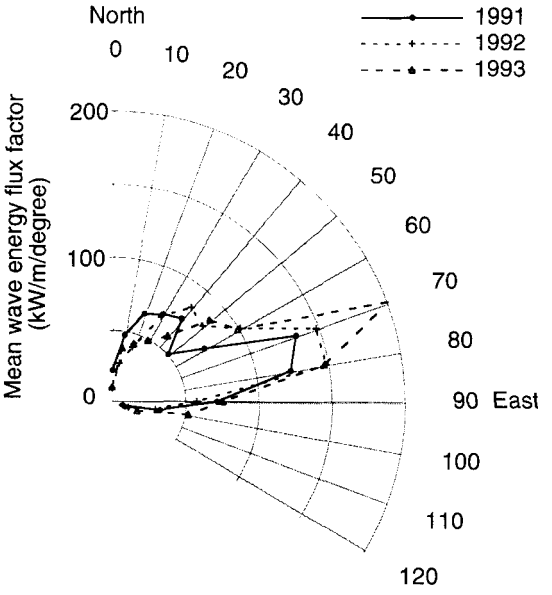

Fig. 9 Directional spread of mean wave energy flux factor for the years 1991–93.

the breaker zone. Positive and negative values of the longshore wave energy flux factor indicate transport to the north-west and south-east, respectively. The plots of the daily averaged values show the direction and magnitude of the transport potential during individual storms, and the cumulative plot of the longshore wave energy flux indicates the net transport potential since the record began.

Comparison of the total and longshore plots shows clearly that not all large storms resulted in large longshore components of wave energy flux. For example, in the July 1992 storm (total energy flux of 100 kW m^{-1}) the longshore component was small (8 kW m^{-1}) because waves arrived from the north-east, almost normal to the coastline. One might expect considerable alteration of the beach profile during such events, but little longshore transport. By comparison, the September 1993 storm had the same total flux (100 kW m^{-1}) but a much larger longshore component (more than 20 kW m^{-1}). This was because the waves approached from the east, at a more oblique angle to the coastline.

A striking feature of Fig. 12 is that the direction of the longshore component changes frequently. This arises because storm waves approach this part of the coast from a range of directions, both north and east of the shore normal. Most of the wave energy from major storms arrived from the east and would have moved sand towards the north-west. This was particularly noticeable during the autumn of 1991, when all major waves arrived from easterly directions and considerable north-westward sand transport should have occurred. The most sustained period of easterly waves occurred through February 1993; however, the storm in September 1993 delivered nearly as much longshore wave energy flux over only 4 days. Fewer high-energy waves arrived from the north (the best example was in May 1993); however, there were long intervals (especially during the 7 months beginning July 1991) when relatively low-energy northerly waves persisted and the littoral transport would have been towards the south-east. Thus there appears to be a broad pattern of energetic episodic north-westwards littoral transport associated with easterly storms and less intense but more persistent reverse transport by northerly waves.

The longshore wave energy flux factor was transformed into a potential longshore sand transport rate using the proportionality coefficient for sand beaches provided by USCERC (1984). Such calculated sand transport rates are potential transport rates only, not directly measured, but derived using several simplifying assumptions. First, the approach used to transform the wave buoy data to the breaker zone assumes that the nearshore contours are parallel. The wave energy fluxes and transport rates estimated in this paper are thus spatially averaged values based on a representative shoreline orientation. This approximation is reasonable for the study location except around the Katikati ebb tidal delta (Hume & Hicks 1993), where the local transport rates can be expected to vary from the average values. Second, it is assumed that the longshore transport is driven only by the longshore component of the wave energy flux. Wind-driven, tidal, and other currents are ignored. The influence of wind-driven currents is uncertain, but apart from around the ebb delta where tidal currents and currents driven by longshore gradients in wave height are locally important, it appears reasonable to ignore the latter sources of current energy because they tend to be minor.

The resulting transport rates, averaged over the 3-year record, were 654 000 $m^3 y^{-1}$ to the north-west and 582 000 $m^3 y^{-1}$ to the south-east. These resolve to a gross transport rate of 1 236 000 $m^3 y^{-1}$

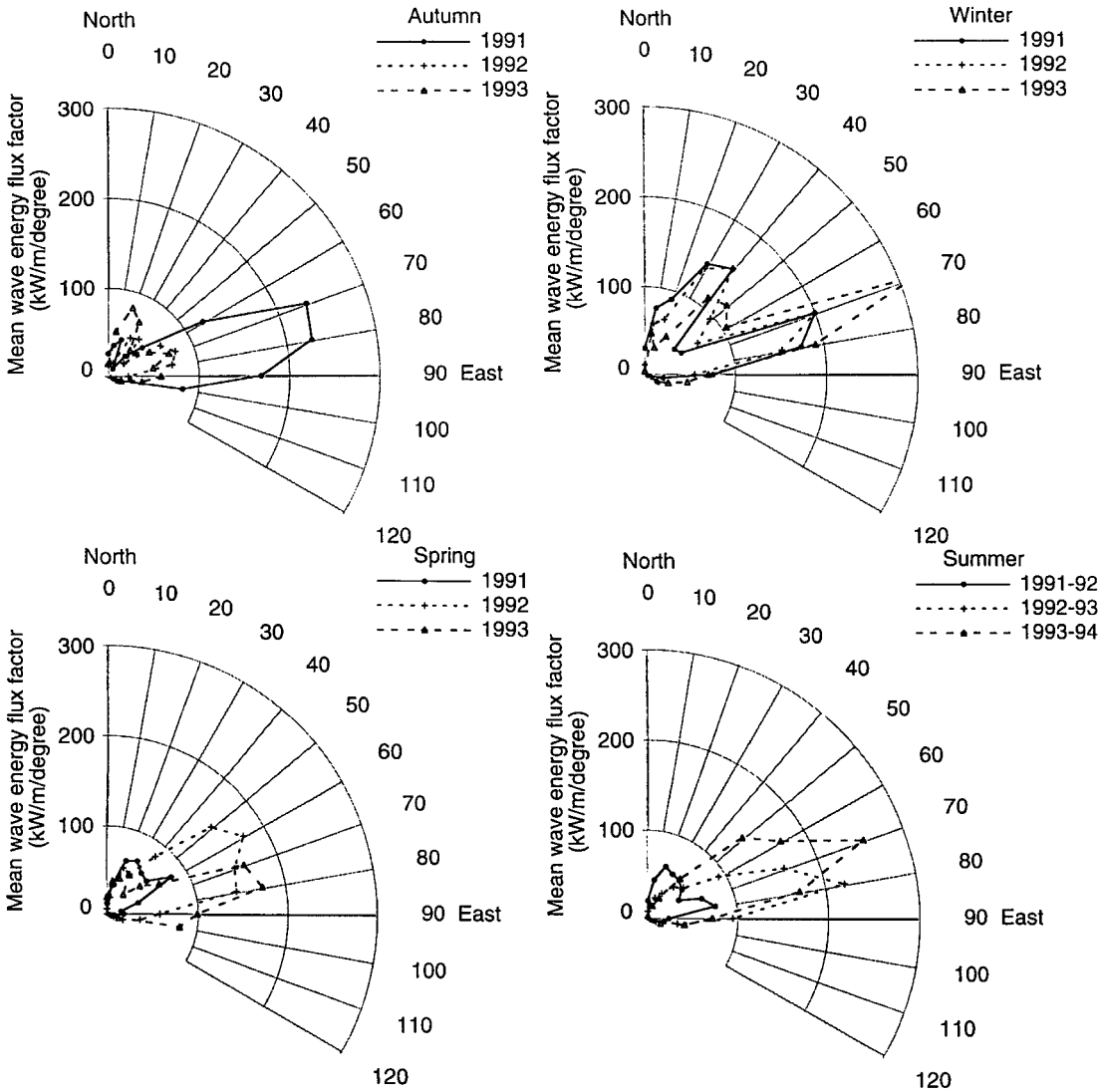

Fig. 10 Directional spread of the mean of wave energy flux factor for individual seasons.

and a net rate of 72 000 $m^3 y^{-1}$ to the north-west. The value of the net transport rate should be regarded with caution, however, since it is established from two large and nearly equal numbers of opposite sign. Thus it is sensitive to errors in the daily transport rates (particularly those due to the orientation assumed for the shoreline) and to the period over which the transport rates are calculated.

Our data indicate that the annual net longshore transport is liable to be variable and small compared to the annual gross longshore transport, and, for any one year, the magnitude and sign of the net transport will depend on the particular mixture of easterly and northerly waves arriving during that year. Harray's (1977) finding, of a net drift towards the south-east at Waihi Beach over an observation period of about a year, is not inconsistent with our results; from July 1991 to October 1992 inclusive the net drift was also south-eastwards, against the overall trend of our 3 years of observations. Harray & Healy (1978) concluded that the net drift is

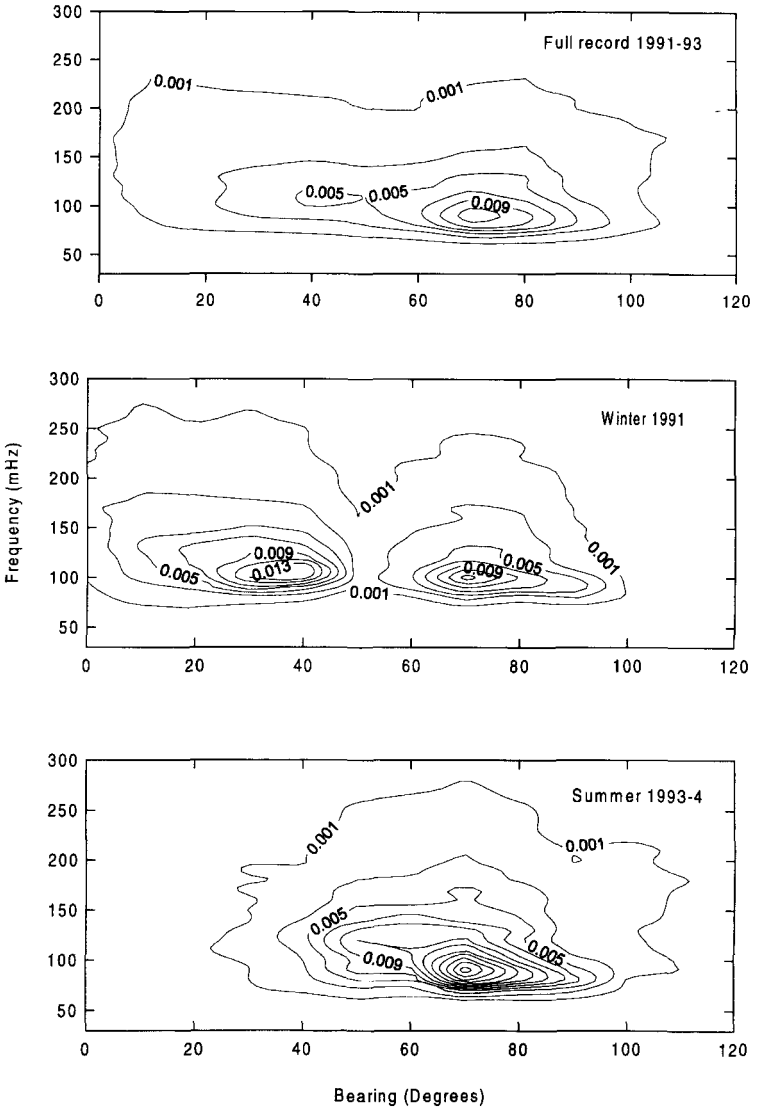

Fig. 11 Two-way distribution of wave energy with frequency and mean wave direction for **A**, the entire three years; **B**, winter 1991; **C**, summer 1993–94. Contour intervals are 0.002 m^{-2} Hz^{-1} $degree^{-1}$.

"clearly south-eastward". However, given the low ratio of net to gross drift, our 3-year observation period is too short to infer a magnitude or even a direction for the long-term net transport along this coast.

Gibb (1979) used sedimentary and geomorphic indicators to infer the direction of net longshore drift. He concluded that net drift near Waihi was south-eastwards and less than 100 000 m^3 y^{-1}, but that east of Tauranga the net drift was in the opposite direction. Given the difficulty in obtaining a wave record representative of the long-term wave climate, identifying those morphological features that reflect long-term trends may offer the best method of detecting any long-term net drift.

DISCUSSION

Comparison with instrument wave measurements at other sites

Great Barrier Island

Waverider measurements were made at a site off the east coast of Great Barrier Island (36°15'S, 175°32'E, see Fig. 1) in 65 m depth for the 2 years 1980–81 (Ewans & Coup 1982; Ewans &

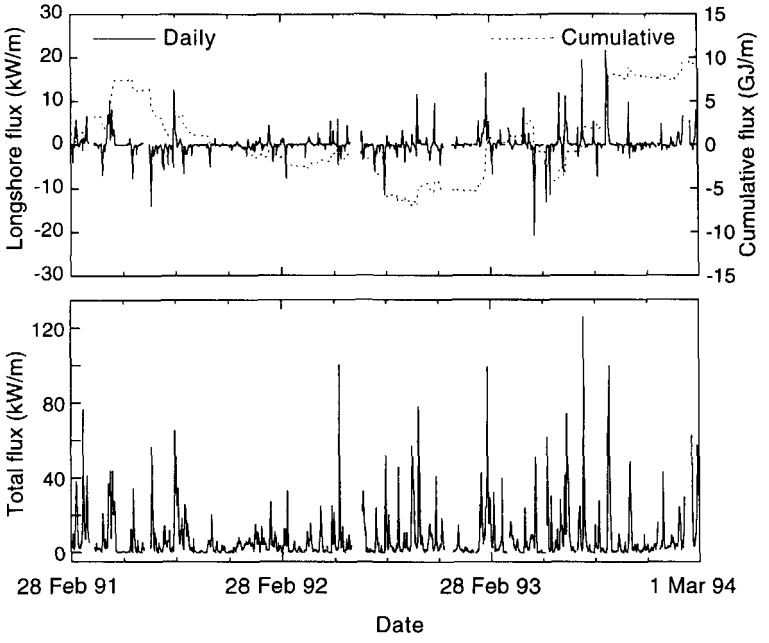

Fig. 12 Daily mean and cumulative longshore wave energy flux factor and total wave energy flux factor, for the period 1991–93.

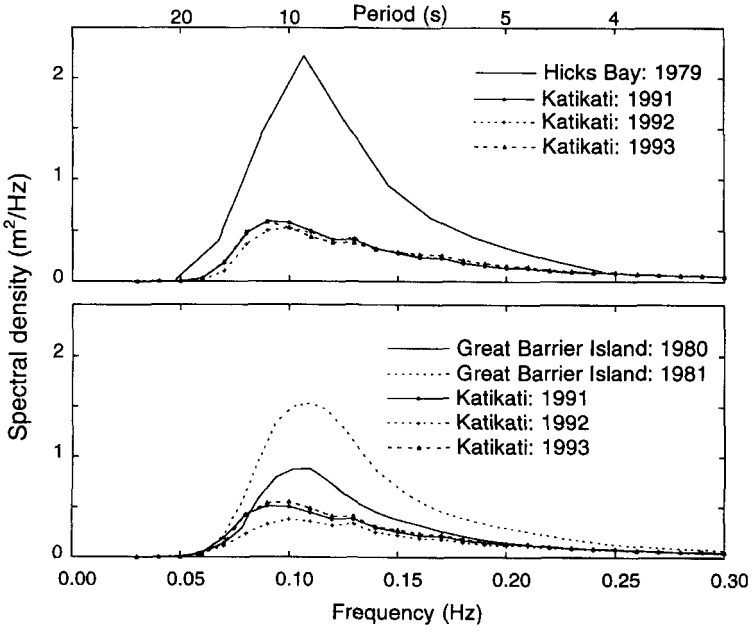

Fig. 13 Spectral energy density for Hicks Bay (1979), Great Barrier Island (1980/81) and Katikati (1991–93).

Kibblewhite 1992). Ewans & Kibblewhite (1992) noted that most of the high-energy events they observed were caused by local easterly winds. They concluded that "a seasonal variation will thus occur as a result of any seasonal variation in the number and intensity of easterly events". The directional data from the present study support that view. The mean annual spectral densities for the Great Barrier Island (1980–81) and Katikati (1991–93) sites are compared in Fig. 13. The Great Barrier Island site

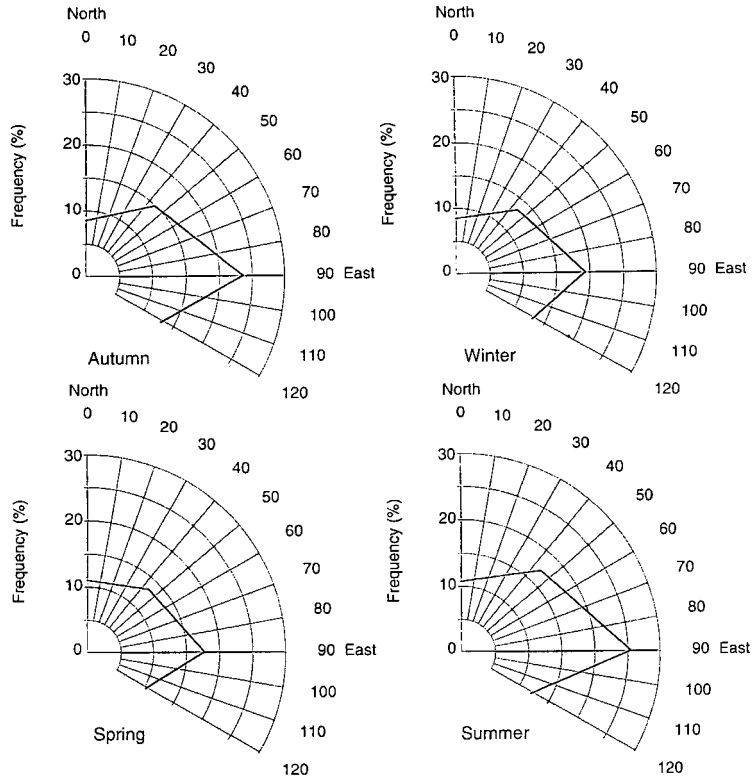

Fig. 14 Directional distribution of swell waves in the Bay of Plenty taken from ships observations (from Reid & Collen 1983).

experienced more than twice the wave energy of the Katikati site. This is to be expected because the Great Barrier Island site is exposed to swells from the east and south-east, whereas the Katikati site is partially sheltered by East Cape. A surprising feature is that spectral peaks for the Great Barrier Island site occur at slightly shorter periods (9–10 s) than those for Katikati (10–11 s): one might have expected the Great Barrier Island site to have experienced more long-period oceanic swells and for the Katikati site to have been sheltered from distant easterly swells by East Cape. Figure 13, therefore, suggests that locally generated wave events are also more severe at the Great Barrier Island site than at Katikati. However, this inference must be treated with caution because the data from the two sites were not collected at the same time.

Hicks Bay

Harris et al. (1983) describe wave measurements made at a deep-water site near Hicks Bay over a 9-month period in March-December 1979. Figure 13 compares the average Hicks Bay spectrum with three spectra calculated at the Katikati site in March-December of 1991, 1992, and 1993. There was about four times more wave energy at Hicks Bay than at the Katikati site and the peak of the Hicks Bay spectrum occurred at a wave period of about 9 s compared with 10–11 s at the Katikati site. Harris et al. (1983) showed that southerly swells reaching the Hicks Bay were much reduced in height by refraction and do not explain the high wave energy at Hicks Bay. They studied synoptic meteorological charts and concluded that most of the wave energy measured at Hicks Bay originated from the north-east quarter, which is also the predominant direction for waves measured at the Katikati site. It is not clear whether the large difference in total wave energy is caused by location or by the different times when data was gathered.

Ship observations

Reid & Collen (1983) summarised the wave records obtained from shipping in 45 different 5° by 5° "squares" around the New Zealand coast for the period 1957–80. These visual records identify long-period "swell" and short-period "wind waves" as separate features. The "square" which covers the

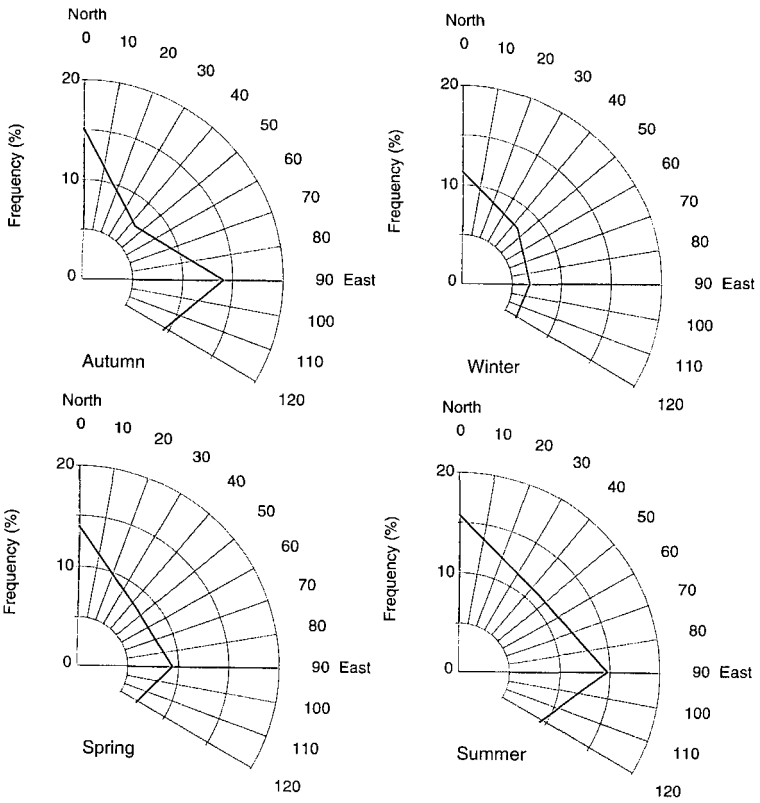

Fig. 15 Directional distribution of wind-generated waves in the Bay of Plenty from ships observations (from Reid & Collen 1983).

Bay of Plenty is centred on 37.5°S, 177.5°E and extends from Whangarei to Hawke Bay. There is a noticeable southerly wave component in the record which would not be expected to affect the Katikati buoy site because of the shelter afforded by the North Island, so in Fig. 14 we have ignored ship reports of waves approaching from the south, south-west, west, and north-west octants. Figure 14 shows a predominant east and north-east "swell wave" characteristic, which is in qualitative agreement with the directional data from the present study (Fig. 10). The directions of "wind waves" vary seasonally (Fig. 15) with on-shore wind waves being more frequent during summer than winter. This implies that there will be more short-period "wind wave" energy at the site in summer, although this trend is not clearly discernible in the present data (Fig. 2, 4, and 8).

Long-term wave climate and the Southern Oscillation Index

Extrapolation of 3 years' data to the long-term wave climate has a considerable statistical uncertainty. To this uncertainty must be added the effect of the Southern Oscillation, which has been identified as a major factor in world weather patterns (see e.g., Philander 1990), and is usually measured using the Southern Oscillation Index (SOI), which is derived from monthly mean sea level pressure at Tahiti and Darwin. The SOI is defined as:

$$SOI = (D-M)/S$$

where D = Tahiti-Darwin difference (hPa) for the month in question, M = Mean Tahiti-Darwin difference; and S = Standard deviation of the monthly Tahiti-Darwin difference. Both M and S are calculated over the base period 1941–80.

Gordon (1985) examined the effect of the SOI on New Zealand weather; he found that negative values of SOI (i.e., El Niño conditions) are associated with anomalous southerly to westerly air flow (the direction varying with the season). The corollary is that La Niña conditions are associated with anomalous northerly to easterly flow. It follows from Gordon's findings that La Niña conditions result in more wave events on the north and east coasts.

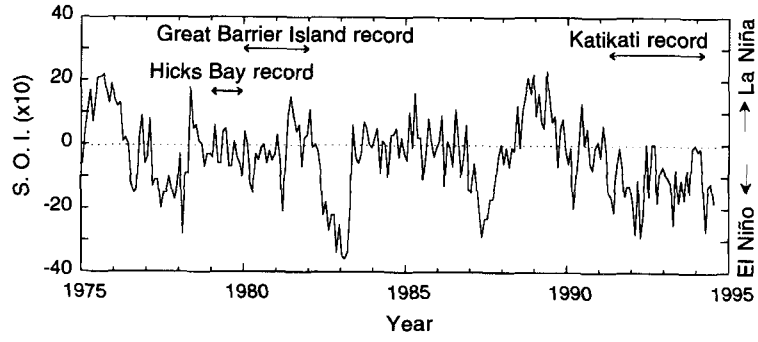

Fig. 16 Variation in the Southern Oscillation Index (1975–93) (pers. comm. B. Mullan, NIWA).

Figure 16 shows the distribution of mean monthly SOI since 1978, from which data it can be seen that the SOI varied from strongly negative to about zero during the 3 years of the present wave record. That means that the more stormy conditions of La Niña do not feature in the record. SOI values for the Great Barrier Island and Hicks Bay records were less strongly negative; 1981 included some La Niña weather. Data have not been recorded from any of the three wave data sites during markedly La Niña conditions.

CONCLUSIONS

At a wave buoy in 34 m water depth in the western Bay of Plenty, significant wave heights were less than 1 m for about 70% of the time and the mean wave heights were about 0.8 m during the 3-year period 1991–93. The highest significant wave height recorded in this time was 4.3 m in June 1992. The peak spectral density of wave energy occurred at periods of 10–11 s. Wave steepness suggests that many of the measured waves originated close to the buoy. The spectral distributions measured at Katikati in 1991–93 are similar to those measured at Great Barrier Island (1980–81) and Hicks Bay (1979) with two differences: at the two latter sites the total energy is greater and T_p is about 9 s. At Katikati there is little difference in average spectral density from year to year but within each year there is considerable variability associated with storm events. Storms can occur at any time of the year but in the recording period there is some evidence of higher wave energy in winter. Most storm wave energy arrived from the north-east to east sector. Spectral peak wave periods during storms ranged from 7.2 to 13.2 s. Periods exceeding 10 s were associated with the sector 50–90° whereas shorter-period waves are incident from north to south-east. Estimates of the longshore component of wave energy flux at the breaker line indicates a broad pattern of north-westwards littoral transport associated with easterly storms and less energetic but more persistent south-eastwards transport driven by northerly waves. The net longshore transport rate (72 000 $m^3 y^{-1}$ north-westwards) was small compared to the gross longshore transport (over 1 000 000 $m^3 y^{-1}$) and fluctuated in direction and magnitude from storm to storm. The Katikati record was measured during El Niño conditions and may not be representative of the long-term wave climate.

ACKNOWLEDGMENTS

This study was funded by the New Zealand Foundation for Research, Science and Technology under contract CO1211. The buoy was deployed and maintained with the assistance of John Nagels, Tony Dolphin, and Rod Budd of NIWA. The Port of Tauranga Ltd assisted by providing facilities for the receiver at Mt Drury. Terry Hume, Murray Hicks, Kit Rutherford, and two anonymous referees reviewed drafts of this paper and made many helpful suggestions.

REFERENCES

Allender, J.; Audunson, T.; Barstow, S. F.; Bjerken, S.; Krogstad, H. E.; Steinbakke, P.; Vartdal, L.; Borgman, L. E.; Graham, C. 1989: The WADIC project: a comprehensive field evaluation of directional wave instrumentation. *Ocean engineering 16*: 505–536.

Christopherson, M. J. 1977: The effect of sand mining on the erosion potential of Whiritoa Beach. Unpublished MSc thesis, University of Waikato, New Zealand. 120 p.

Davies-Colley, R. J. 1976: Sediment dynamics of Tauranga Harbour. Unpublished MSc thesis, University of Waikato, New Zealand. 148 p.

de Lange, W. 1991: Wave climate for No. 1 Reach, Port of Tauranga, Tauranga Harbour, Report to the Port of Tauranga Ltd, September 1991, Marine Geosciences Group, University of Waikato, New Zealand, 18 p.

Ewans, K. C.; Kibblewhite, A. C. 1992: Spectral features of the New Zealand deep-water ocean wave climate. *New Zealand journal of marine and freshwater research 26*: 323–338.

Ewans, K. C.; Coup, D. B. 1982: A spectral history of the ocean wave field off the East Coast of Great Barrier Island. Maui Development Environmental Study, Phase II. University of Auckland Report 82–11.

Gibb, J. G. 1979: Aspects of beach sediments and their transport along the New Zealand coast. *In*: Workshop–Physical aspects of coastal problems, Hamilton, 11–12 October, unpublished proceedings, Ministry of Works & Development.

Gordon, N.D. 1985: The Southern Oscillation and New Zealand weather, *Monthly weather review, 114*: 371–387.

Harray, K. G. 1977: Beach erosion and sediments at Waihi Beach. Unpublished MSc thesis, University of Waikato, New Zealand.

Harray, K. G.; Healy, T.R. 1978: Beach erosion at Waihi Beach. *New Zealand journal of marine and freshwater research 12*: 99–107.

Harris, T. F. W.; Hughes, T. S.; Valentine, E. M. 1983: Deepwater waves off Hicks Bay and the Northeast Coast, North Island. *Water & Soil miscellaneous publication 56*. 83 p.

Hume, T. M.; Bell, R. G.; de Lange, W. P.; Healy, T. R.; Hicks, D. M.; Kirk, R. M. 1992: Coastal oceanography and sedimentology in New Zealand, 1967–91. *New Zealand journal of marine and freshwater research 26*: 1–36.

Hume, T. M.; Hicks, D. M. 1993: Shelf morphology and processes near an ebb tidal delta, Katikati Inlet, New Zealand. *In*: Proceedings of the 11th Australasian Conference on Coastal and Ocean Engineering, Townsville, 23–27 August. Institution of Engineers Australia: 671–676.

Philander, S.G.H. 1990: El Niño, La Niña and the Southern Oscillation. Academic Press.

Pickrill, R. A.; Mitchell, J. S. 1979: Ocean wave characteristics around New Zealand. *New Zealand journal of marine and freshwater research 13*: 501–520.

Reid, S. J.; Collen, B. 1983: Analyses of wave and wind reports from ships in the Tasman Sea and New Zealand areas. *New Zealand Meteorological Service miscellaneous publication 182*.

USCERC. 1984: Shore Protection Manual 4th Edition, Department of the Army Corps of Engineers, Virginia. U.S. Coastal Engineering Research Centre.

APPENDIX I

Definition of wave parameters used in this report.

Significant wave height H_s

This wave height is considered to approximate the height that a visual observer might estimate and can be calculated two ways:

(1) as originally defined: the average of the highest one-third of the waves, where each wave begins and ends at a negative zero crossing, and its height is measured from the lowest trough to the highest crest; and

(2) in the frequency domain, as $H_s = 4\,\sigma$ (see under "Mean Wave Direction" for a definition of σ).

In this paper the first of these definitions has been used.

Significant wave period T_s is defined in the Shore Protection Manual (USCERC 1984) as the average period (between zero-crossings) of the highest one-third of the waves. T_s is thus longer than the zero-crossing wave period T_z (see below).

Zero-crossing wave period T_z is the average period, measured between negative zero crossings, of **all** the waves.

Spectral peak period T_p is the period corresponding to the maximum spectral density.

Spectral density

The vertical displacement of the water surface, $n(t)$, can be represented by a Fourier Series:

$$n(t) = \sum_{j=1}^{N} a_j \cos\left(\omega_j t - \phi_j\right)$$

where the i^{th} Fourier component has a magnitude a_i, angular velocity ω_i, and phase ϕ_i.

Then we may define the spectral density $E(\omega_j)$ by

$$E(\omega_j) = \frac{a_j^2}{2\Delta\omega}$$

where $\Delta\omega = \omega_{j+1} - j\omega_j$

The spectral density is proportional to the wave energy and is therefore often referred to as the energy density.

Mean wave direction has been calculated using the mean direction, $\theta(\omega_j)$, of each frequency bandwidth:

$$\theta_{mean} = \sum_{j=1}^{N} E(\omega_j)\,\theta(\omega_j)/\sigma^2$$

where

$$\sigma^2 = \sum_{j=1}^{N} E(\omega_j)$$

Wave energy flux factors

At the buoy the total wave energy flux factor per unit length of wave crest (USCERC 1984) can be calculated using an equation on p. 4.92 of the Shore Protection Manual.

$$P = (\rho\, g\, H_s^2\, C_g)/8$$

where H_s is the significant wave height and C_g is the group velocity. In this report, the deepwater value of C_g has been substituted (a reasonable approximation at the buoy site) to obtain:

$$P = \rho\, g^2\, H_s^2\, T_p/(32\,\pi).$$

The total wave energy flux factor per unit length of coastline is specified on p. 4.92 of the Shore Protection Manual as $P \cos\alpha$, where α is the angle between the wave crest and the shoreline. For the present site $\alpha = \theta_{mean} - 59°$. The coastline flux then becomes:

$$P \cos\alpha = \rho\, g^2\, H_s^2\, T_p \cos\alpha/(32\,\pi)$$

Longshore wave energy flux factor

Equation 4–45 of the Shore Protection Manual was used to estimate the longshore energy flux factor, P_{ls}, which is often used in calculations of longshore sediment transport rate:

$$P_{ls} = 0.05\,\rho\, g^{3/2}\, H_{so}^{5/2}\,(\cos\alpha_o)^{1/4} \sin 2\,\alpha_o$$

where H_{so} is the significant wave height in deep water and α_o is the angle between the deep water wave crest and the shoreline. Use of this formula assumes that sea bed contours are parallel to the coastline in regions where refraction occurs. This condition is met in the preset uses. Refraction calculations to determine H_{so} and α_o from conditions at the buoy have also assumed that bed contours are parallel to the coastline.

Note that P, $P \cos\alpha$ and P_{ls} are correctly termed "wave energy flux factors", rather than actual wave energy fluxes. This is because H_s has been used to characterise wave height (see USCERC 1984: 4–93).